

# Fabrication and Characterization of Electrodeposited Bismuth Telluride Films and Nanowires

Cheng-Lung Chen,<sup>†,‡</sup> Yang-Yuan Chen,<sup>\*,‡</sup> Su-Jien Lin,<sup>\*,†</sup> James C. Ho,<sup>‡,§</sup> Ping-Chung Lee,<sup>‡</sup> Chii-Dong Chen,<sup>‡</sup> and Sergey R. Harutyunyan<sup>‡,||</sup>

Department of Materials Science and Engineering, National Tsing Hua University, Hsinchu, Taiwan, Republic of China, Institute of Physics, Academia Sinica, Taipei, Taiwan, Republic of China, and Institute for Physical Research, NAS, Ashtarak-2, Armenia

Received: October 16, 2009; Revised Manuscript Received: January 25, 2010

To elucidate low-dimensional effects on thermoelectric materials, bismuth telluride film and nanowires array were fabricated by potentiostatically electrodeposition. Both materials are slightly Te-rich, n-type Bi<sub>2</sub>Te<sub>3</sub>, exhibiting preferred orientation in rhombohedral structure. For both the Seebeck coefficient  $S \approx -70 \mu\text{V/K}$  at 300 K decreases linearly with decreasing temperature, showing a diffusive nature of current flow. The temperature dependence of resistivity ( $=1/\sigma$ ) of nanowires obtained from the data of a nanowires array and a single-nanowire reveals a better electric conductivity than that of the bulk. By coupling temperature-dependent thermal diffusivity and heat capacity data with a modified effective medium theory, a thermal conductivity  $\kappa$  of 0.75 W/(m K) was obtained at 300 K. The ZT was calculated to be 0.45 at 300 K and 0.9 at 350 K for Bi<sub>2</sub>Te<sub>3</sub> nanowires.

## 1. Introduction

Thermoelectric (TE) materials are capable of converting thermal energy directly into electrical energy or vice versa, as being demonstrated in power generation or refrigeration. However, low efficiency has limited their use only in niche markets.<sup>1,2</sup> The efficiency of a thermoelectric material is conventionally judged by its dimensionless figure of merit,

$$ZT = \sigma S^2 T / \kappa \quad (1)$$

where  $T$ ,  $S$ ,  $\sigma$ , and  $\kappa$  are respectively the absolute temperature, Seebeck coefficient, electrical conductivity, and thermal conductivity.<sup>3</sup> The compound parameter,  $\sigma S^2$ , is often referred to as the power factor. Accordingly, an ideal TE material should possess high Seebeck coefficient, high electrical conductivity, but low thermal conductivity, a requirement not easily met. Over the years, bismuth telluride, Bi<sub>2</sub>Te<sub>3</sub>, has been recognized as the best TE material with the highest  $ZT \approx 1$  near ambient temperature.<sup>4</sup> To enhance future applications, the ZT value needs to be further raised considerably. A seemingly viable approach is reduction of dimensionality. For example, a ZT enhancement mainly due to thermal conductivity reduction, through phonon-blocking and electron-transmitting, in superlattices was reported by Venkatasubramanian et al.<sup>5</sup> Much higher ZT values were even predicted theoretically by Hicks and Dresselhaus for one-dimensional, nanowire wires, based on the change of electronic density-of-states and increased phonon surface scattering.<sup>6</sup> This work is, therefore, carried out as part of our targeted efforts to elucidate low-dimensional effects on  $S$ ,  $\sigma$ , and  $\kappa$ .

Many techniques including coevaporation, molecular-beam epitaxy, and metal–organic chemical vapor deposition have

been developed to grow Bi<sub>2</sub>Te<sub>3</sub> films.<sup>7–9</sup> Even though they are capable of producing good quality films, the high fabrication cost and toxic precursors make them impractical in large scale production. An alternative method is chemical electrodeposition, which is also applicable to fabricate nanowires in prepatterned templates.<sup>10,11</sup> Nanoporous membranes such as anodized aluminum matrix (AAM) can be used as the template material, since they are particularly suitable for preparing high aspect ratio structures. Due to its inherent advantages of simplicity, rapidity, and cost-effectiveness, this method has been extensively applied to many thermoelectric materials including some based on bismuth telluride.<sup>12–15</sup> Even so, a comprehensive understanding of thermoelectric properties at low dimensions remains as the ultimate goal in obtaining high ZT materials.

While certain growth conditions for films have been reported recently,<sup>16</sup> thermoelectric transport property data are somewhat limited. In this respect, fabricating a thermoelectric device based on nanowires is even more an arduous task, considering the dissonant gap between synthesis and thermoelectric characterization of the product. Furthermore, most of the electrodeposition baths were developed first for thin films and then demonstrated for nanowires by filling the nanoporous membrane. In this article, we present a systematic study of potentiostatically electrodeposited Bi<sub>2</sub>Te<sub>3</sub> films and nanowires embedded in AAM. Electrical resistivity and Seebeck coefficient were directly measured. An indirect but viable approach is introduced to conveniently characterize thermal conductivity of nanowires. This was done by coupling experimentally determined thermal diffusivity and heat capacity data with a modified effective medium theory. Finally, the individual parameters  $S$ ,  $\sigma$ , and  $\kappa$  together result in estimated ZT values.

## 2. Experimental Section

Bi<sub>2</sub>Te<sub>3</sub> films were electrodeposited potentiostatically at  $-150$  mV onto an ITO glass substrate from 1 M HNO<sub>3</sub> solution containing 0.008 M Bi<sup>3+</sup> and 0.014 M HTeO<sub>2</sub><sup>+</sup>. The overall chemical reaction can be described as<sup>17</sup>

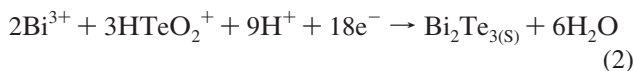
\* To whom correspondence should be addressed. E-mail: chenyl2@phys.sinica.edu.tw (Y.Y.C.) and sjlin@mx.nthu.edu.tw (S. J. L.).

<sup>†</sup> National Tsing Hua University.

<sup>‡</sup> Academia Sinica, Taipei.

<sup>§</sup> On leave from Wichita State University, Wichita, Kansas.

<sup>||</sup> Institute for Physical Research, NAS.



The process was carried out in a conventional three-electrode cell with a saturated calomel electrode as the reference and a platinum sheet as the counter electrode. To remove oxygen from solution, argon was bubbled into the electrolyte throughout the experiment. After electrodeposition, as-prepared  $\text{Bi}_2\text{Te}_3$  films were annealed in argon with 5%  $\text{H}_2$  at 523 K for 2 h.

The AAM template was produced in a two-step anodized process.<sup>18</sup> An aluminum foil with purity 99.999% and thickness 0.13 mm (Alfa Aesar) was anodized in acid solutions, yielding an array of densely packed, hexagonally arranged, parallel nanochannels. The channel diameter can be systematically controlled by anodized voltage, type of electrolyte, and bath temperature. After anodization, the remaining aluminum layer was removed by  $\text{CuCl}_2$  solution. A subsequent etching treatment by 0.5 M  $\text{NaOH}$  aqueous solution for 7–10 min was carried out to remove the barrier layer on the bottom side, followed by depositing a gold-film layer to serve as a conductive electrode.

By filling the template, a  $\text{Bi}_2\text{Te}_3$  nanowires array was then fabricated with similar growth conditions, rinsed with deionized water, and dried in nitrogen. A thin gold film (~300 nm) was thermally evaporated onto the top surface for oxidation prevention. It has been suggested that annealing treatment to nanowires would improve their thermoelectric properties.<sup>19</sup> In our experience, annealing lowers electrical resistivity of as-prepared film as expected, but the annealing-induced thermal shock leads to extremely high electrical resistance in nanowires embedded in AAM. Therefore, experimental data and analysis were confined to  $\text{Bi}_2\text{Te}_3$  bulk, annealed films, and as-prepared nanowires. To obtain individual nanowires, AAM was dissolved in 2 M  $\text{NaOH}$  aqueous solution, then washed by deionized water and centrifuged to remove residual  $\text{NaOH}$  thoroughly. Separated  $\text{Bi}_2\text{Te}_3$  nanowires were dispersed in ethanol, ready for measurements.

For comparison with films and nanowires, a  $\text{Bi}_2\text{Te}_3$  bulk was prepared by the Bridgeman method. Briefly, high-purity (99.999%) bismuth and tellurium powders were mixed in the appropriate molar ratio and sealed in a quartz tube, which was evacuated to  $10^{-5}$  Torr, kept in a furnace at 1073 K for 12 h, and then cooled to room temperature in 1 day.

A 3-KW diffractometer (Philips) equipped with an array detector based on real time multiple strip was employed for crystal structural characterization. Morphologies of films and nanowires array were determined by a field emission scanning electron microscope (SEM, Hitachi S-4200), and compositions by energy dispersive X-ray. Transmission electron micrographs (TEM) and diffraction patterns were obtained with a field emission transmission electron microscope operated at 200 kV (JEOL JEM-2100).

A standard four-probe resistivity measurement was performed on  $\text{Bi}_2\text{Te}_3$  bulk, films, and nanowires with a physical property measurement system (Quantum Design). However, for nanowires array, gold layers were first deposited on the two sides of array employed as electric contacts of the four-probe method. Measurements of Seebeck coefficient between 120 and 350 K were performed by a longitudinal DC steady-state method on specially designed setups for film (Figure 1a) and nanowires (Figure 1b), with  $S = \Delta V/\Delta T$ , where  $\Delta T$  is the temperature gradient across the sample, and  $\Delta V$  is the thermo-emf generated by  $\Delta T$ . At a given temperature, a programmable power supply was controlled by the LABVIEW graphical program to develop a small temperature gradient across the sample. Typically,  $\Delta T$  is set in the range of 0.5–1 K monitored by a pair of T-type thermocouples. The

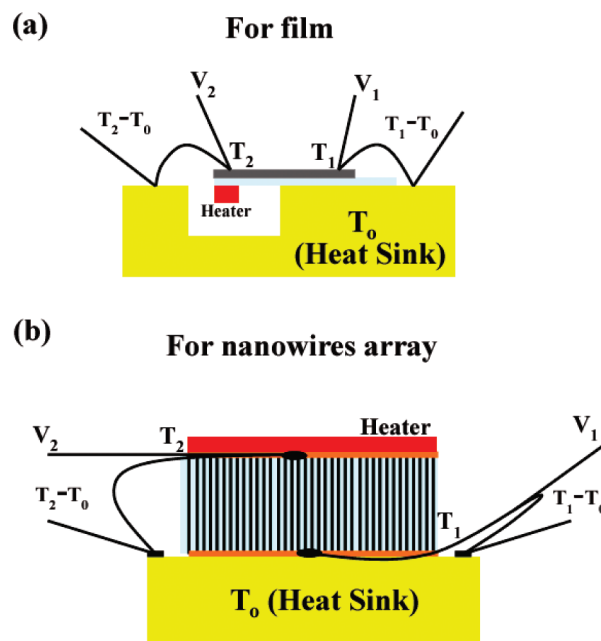


**Figure 1.** Schematic setup for the Seebeck coefficient measurements on (a) film and (b) nanowires array in AAM.

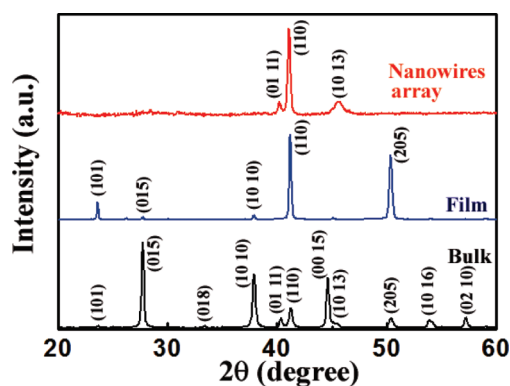


**Figure 2.** X-ray diffraction patterns for  $\text{Bi}_2\text{Te}_3$  bulk, annealed film, and as-prepared nanowires array.

resulting thermo-emf  $\Delta V$  was continuously recorded by a digital voltmeter. By varying  $\Delta T$ , a statistically averaged  $S$  value was derived from the slope of a  $\Delta V$  vs  $\Delta T$  plot.

Thermal diffusivity measurements were carried out with use of laser flash equipment (LFA 457, NETZSCH) on flat disk samples.<sup>20</sup> Briefly described, the front side of the specimen was heated by a short pulse of an Nd:YAG laser. The temperature on the opposite side was measured by an infrared detector. The measured exothermic curve and laser pulse shape were evaluated by a fitting procedure.<sup>21,22</sup> Before each measurement, a piece of ultrapure iron (99.999%) was used as a standard to ensure the reliability of the equipment. A differential scanning calorimeter (Q 100, TA Instruments) was employed for heat capacity measurements.

### 3. Results and Discussion

**3.1. Morphology and Structure.** X-ray diffraction patterns for  $\text{Bi}_2\text{Te}_3$  bulk, annealed film, and as-prepared nanowires array are presented in Figure 2. All peaks can be indexed to those of rhombohedral structure ( $R\bar{3}m$ ), confirming their single-phase purity.<sup>23</sup> The strong (110) peak suggests that the  $c$ -axis is parallel to the film surface and perpendicular to the axis of the nanowire, respectively. Figure 3 shows the morphology of as-prepared and

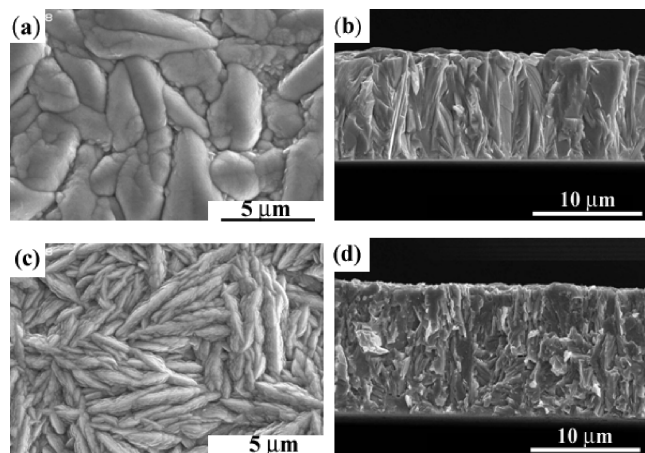


**Figure 3.** Scanning electron micrographs of  $\text{Bi}_2\text{Te}_3$  films: (a) planar and (b) cross-sectional view of as-prepared film and (c) planar and (d) cross-sectional view of annealed film.

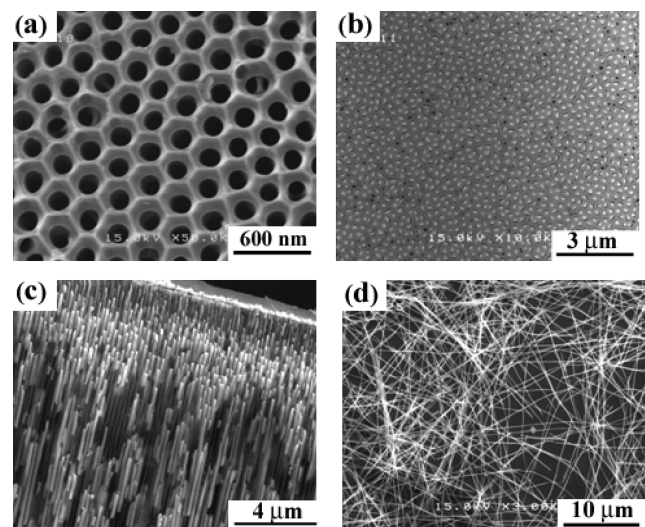


**Figure 4.** Scanning electron micrographs of AAM and  $\text{Bi}_2\text{Te}_3$  nanowires array. (a) Highly ordered nanopores in AAM. (b) Top view of  $\text{Bi}_2\text{Te}_3$  nanowires array. (c) Side view of  $\text{Bi}_2\text{Te}_3$  nanowires array partially embedded in AAM. (d) Separated nanowires after AAM being dissolved.

annealed  $\text{Bi}_2\text{Te}_3$  films. Obviously, annealing yields formation of nanocrystalline structures. The scanning electron micrographs suggest a nucleation-and-growth mechanism on the surface of the substrate. Figure 4a reveals hexagonally ordered nanochannels in AAM. The approximately 120-nm pore diameter then would be that of  $\text{Bi}_2\text{Te}_3$  nanowires. Figure 4b is a mechanically polished top view of the AAM template after being deposited with  $\text{Bi}_2\text{Te}_3$ . Only a few pores remain blank. The same conclusion can be made from the side view in Figure 4c, where most of the pores are filled with  $\text{Bi}_2\text{Te}_3$ . The filling ratio and porosity of the template are estimated to be about 88% and 25%, respectively, comparable to the best samples of this kind ever reported.<sup>24</sup> Separated nanowires in Figure 4d were obtained after AAM was dissolved by aqueous NaOH. Most of them have lengths longer than 20  $\mu\text{m}$ . Judging from energy dispersive X-ray analysis, the only elements present in both films and nanowires are Bi and Te in a ratio of 0.37:0.63, corresponding to Te-rich n-type  $\text{Bi}_2\text{Te}_3$ . Extra Te may be situated as substitution to Bi sites or at interstitial sites. They may also be in grain boundaries, but not enough to be observed in XRD as an impurity phase.<sup>25</sup>

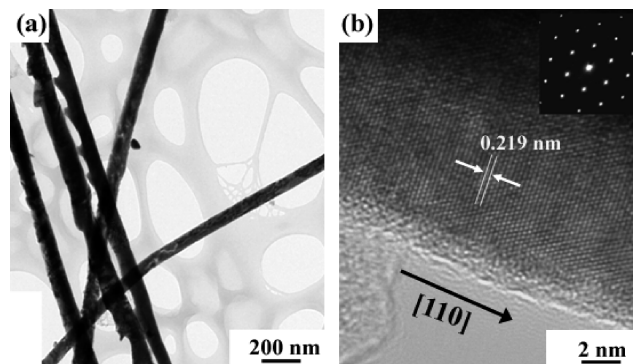


**Figure 5.** (a) TEM image of  $\text{Bi}_2\text{Te}_3$  nanowires. (b) HRTEM image of a single  $\text{Bi}_2\text{Te}_3$  nanowire. Inset: Diffraction patterns of a selected area.

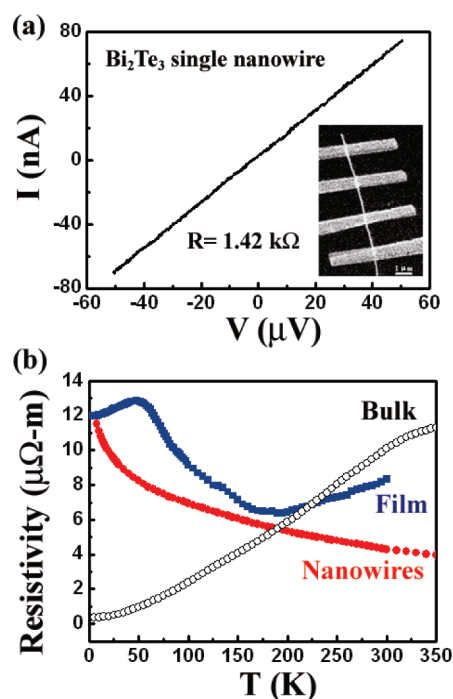


**Figure 6.** (a)  $I$ - $V$  curve of single nanowire at 300 K. Inset: SEM image of four-probe setup. (b) Temperature dependence of electrical resistivity for bulk, annealed film, and as-prepared nanowires array.

The TEM image in Figure 5a reveals the uniform profile of nanowires. A typical high-resolution TEM (HRTEM) image of a single  $\text{Bi}_2\text{Te}_3$  nanowire, along with electron diffraction patterns from a selected area, is given in Figure 5b. Lattice fringes yield an interplanar distance of about 0.219 nm, consistent with the interplanar spacing of the {110} planes of rhombohedral  $\text{Bi}_2\text{Te}_3$  bulk. This result confirms the direction of the long axis of the nanowire is [110].

**3.2. Electric Resistance and Resistivity.** Electrical conductivity  $\sigma$  in eq 1 is the inverse of electrical resistivity, which can be derived from experimentally determined resistivity. The temperature dependence of resistance of nanowires array shows a much larger value than that expected, indicating that most of the nanowires have broken midsections inside the template. To obtain intrinsic electrical resistivity of nanowires, we set up a measurement on a single nanowire separated from the array at 300 K, as shown in the inset of Figure 6a. E-beam lithography and thermal evaporation techniques were applied to fabricate four nickel electrodes onto a 120-nm diameter and 3.7- $\mu\text{m}$  long nanowire. The perfectly linear current-voltage curve in Figure 6a yields a resistance of 1.42 k $\Omega$ . The corresponding resistivity

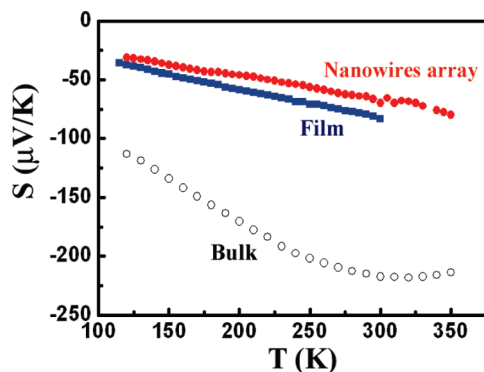


**Figure 7.** Temperature dependence of the Seebeck coefficient of  $\text{Bi}_2\text{Te}_3$ : bulk, annealed film, and as-prepared nanowires array.

of  $4.3 \mu\Omega\cdot\text{m}$  is smaller than  $19 \mu\Omega\cdot\text{m}$  of stoichiometric bulk  $\text{Bi}_2\text{Te}_3$ .<sup>3</sup> This is somewhat expected for our Te-rich composition. According to Fleurial et al., the electrical resistivity of n-type bulk single-crystal  $\text{Bi}_2\text{Te}_3$  decreases toward a low value of  $2 \mu\Omega\cdot\text{m}$  with increasing Te content.<sup>26</sup> Meanwhile, theoretical studies also show that any vacancy, antistructural defects, and substitutional defects will produce higher polarization in bonding between the defect and neighboring atoms, thereby contributing extra charges to conduction.<sup>27,28</sup> Figure 6b summarizes the temperature dependence of resistivity of each sample between 5 and 350 K. The film has its 300 K resistivity reduced considerably through annealing to  $8.3 \mu\Omega\cdot\text{m}$  from  $47.5 \mu\Omega\cdot\text{m}$  in the highly disordered, as-prepared condition. It also displays complex temperature dependence, likely reflecting the interplay between semiconducting and semimetallic character. Indeed, even the normally semimetallic  $\text{Bi}_2\text{Te}_3$  in the bulk form can become semiconducting by changing synthesis conditions or relative contents between Bi and Te.<sup>29,30</sup> Furthermore, the highly anisotropic structure could have different electronic and transport behaviors in different directions. Their different temperature dependence could likely contribute to the observed slope change at 200 and again at 50 K.

The resistivity of a nanowires array plotted in Figure 6b was normalized by the magnitude of a single nanowire measured at 300 K. In contrast to the bulk, a semiconducting-type behavior prevails in the nanowires array. Its resistivity, along the nanowire axis, follows an exponential temperature dependence. This observation, however, disagrees with theoretical calculations, which result in a positive temperature dependence of resistivity for polycrystalline  $\text{Bi}_2\text{Te}_3$  nanowires.<sup>31</sup> The discrepancy is not surprising, considering the off-stoichiometry and high degree of disorder in the as-prepared nanowires. In fact, such variations in resistivity are often characteristic of nanocrystalline materials, which possess different degrees of disorder and formation of grain boundary barriers in microstructure.<sup>32</sup>

**3.3. Seebeck Coefficient.** Seebeck coefficient data are essential to evaluate thermoelectric materials. Figure 7 shows the temperature dependence of Seebeck coefficients of  $\text{Bi}_2\text{Te}_3$  bulk, annealed films, and as-prepared nanowires from 120 to 350 K. The absolute value of  $S$  decreases almost linearly with decreasing temperature, demonstrating the diffusive nature of current flow. Comparable results have been previously reported.<sup>33</sup>

In the two-band model,  $S = (\sigma_e S_e + \sigma_h S_h) / (\sigma_e + \sigma_h)$ , where the subscripts e and h of electrical conductivity  $\sigma$  refer to electrons and holes, respectively.<sup>34</sup> For as-prepared films and nanowires along the nanowire axis,  $S \approx -65 \mu\text{V}/\text{K}$  at 300 K, the negative sign points to electrons as majority carriers and the material as an n-type semiconductor. This relatively low

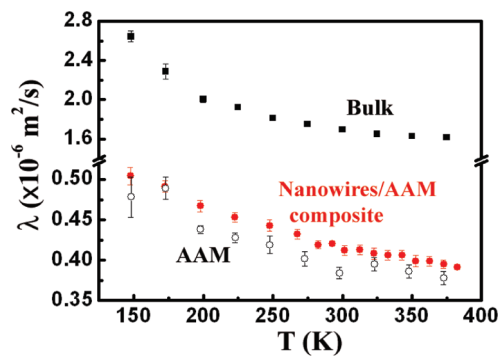


**Figure 8.** Temperature dependence of thermal diffusivity of unfilled AAM and  $\text{Bi}_2\text{Te}_3$ : bulk and nanowires/AAM composite.

value, being less than half of that of bulk, was probably a consequence of structural imperfections and excess Te in electrodeposited, nanocrystalline materials. Structural imperfections caused by antisite defects<sup>28</sup> and additional Te are able to contribute more carrier concentration. There is often an optimal value of charge carrier density at which the Seebeck coefficient is maximum.<sup>35</sup> Higher carrier concentration due to defects would result in a lower Seebeck coefficient. Our electrical resistivity data also suggest that the carrier concentration is likely beyond the optimal value and leads to a lower Seebeck coefficient. Annealing of as-prepared films has been shown to be capable of reducing structural defects, as demonstrated by the significant reduction of electrical resistance. However, it raises the Seebeck coefficient of films only slightly from  $-65$  to  $-80 \mu\text{V}/\text{K}$  at 300 K, suggesting that the type of defects critical to  $S$  cannot be simply improved by annealing. Nevertheless, using resistivity and Seebeck coefficient data thus obtained from annealed film, a power factor ( $\sigma S^2$ ) of  $860 \mu\text{W}/(\text{m K}^2)$  at 300 K is derived. This value sits among those of best electrodeposited films. In the as-prepared nanowires, the power factor is estimated to be  $\sim 1000 \mu\text{W}/(\text{m K}^2)$ , about 15% superior to that of annealed film.

**3.4. Thermal Conductivity and Figure of Merit.** Instead of direct measurements, thermal conductivity can normally be determined from the equation

$$\kappa = \lambda \rho C_p \quad (3)$$

where  $\lambda$ ,  $\rho$ , and  $C_p$  are thermal diffusivity, density, and heat capacity, respectively, of a given sample. In turn, thermal diffusivity was measured with a laser flash apparatus (NETZSCH). Experiments on film were not successful, because it is too thin and fragile to be fitted in the measuring setup. Other results are summarized in Figure 8. For bulk  $\text{Bi}_2\text{Te}_3$ , the various parameters ( $\lambda = 1.69 \times 10^{-6} \text{ m}^2/\text{s}$ ,  $\rho = 7.70 \text{ g}/\text{cm}^3$ , and  $C_p = 0.16 \text{ J}/(\text{g K})$ ) yield  $\kappa = 2.08 \text{ W}/(\text{m K})$  at 300 K. Similarly, for unfilled AAM template along the channel axis ( $\lambda = 0.38 \times 10^{-6} \text{ m}^2/\text{s}$ ,  $\rho = 3.35 \text{ g}/\text{cm}^3$ , and  $C_p = 0.77 \text{ J}/(\text{g K})$ ),  $\kappa = 0.98 \text{ W}/(\text{m K})$  at 300 K. Both  $\kappa$  values are reasonable, thus assuring the validity of the measurement technique. When it is applied to nanowires/AAM composite along the nanowire axis, a  $\lambda$  of  $0.41 \times 10^{-6} \text{ m}^2/\text{s}$  at 300 K was obtained, which is slightly higher than that of the unfilled AAM template, but only about one-fourth of the bulk value. Unfortunately, from this result one cannot generate the thermal conductivity of the nanowires alone. To overcome this difficulty, we employ an alternative approach based on a modified effective medium theory model.<sup>24,36</sup> In this model,

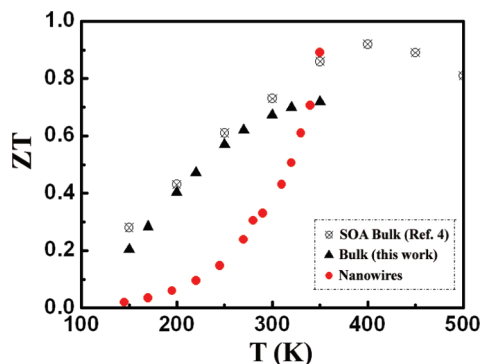


**Figure 9.** Temperature dependence of ZT for nanowires and bulks.

thermal diffusivity of the composite  $\lambda_{\text{NW+AAM}}$  along the nanowire axis has the following dependence on various parameters of  $\text{Bi}_2\text{Te}_3$  nanowires and AAM, respectively:

$$\lambda_{\text{NW+AAM}} = \frac{(1 - \Phi)\kappa_{\text{AAM}} + \Phi\kappa_{\text{NW}}}{(1 - \Phi)(\rho C_p)_{\text{AAM}} + \Phi(\rho C_p)_{\text{NW}}} \quad (4)$$

The percentage of nanowires in the composite,  $\Phi \approx 25\%$ , was estimated by the cross-sectional areal ratio of nanowires to the whole composite, based on SEM images. The diameter of nanowires ranges between 110 and 135 nm, with an average of about 120 nm. If we assume that nanowires have the same properties as those of bulk, the calculated thermal diffusivity  $\lambda_{\text{NW+AAM}}$  of  $0.56 \times 10^{-6} \text{ m}^2/\text{s}$  from eq 4 would obviously be overestimated as compared to the measured value of  $0.41 \times 10^{-6} \text{ m}^2/\text{s}$  at 300 K. To make the two numbers match, we arrive at a smaller  $\kappa = 0.75 \text{ W}/(\text{m K})$  for nanowires, which is about one-third of that of bulk. The considerable reductions in thermal conductivity for nanowires were also observed in other work.<sup>37,38</sup> Then, for a single nanowire with the same  $\kappa = 0.75 \text{ W}/(\text{m K})$  and a power factor of  $1000 \mu\text{W}/(\text{m K}^2)$ , an estimated figure of merit ZT can be obtained as 0.45 at 300 K.

Finally, temperature dependence of the figure of merit for nanowires between 150 and 375 K in Figure 9 was derived from measured  $S$ ,  $\sigma$ , and  $\kappa$  at each given temperature  $T$ . As compared to the state-of-the-art (SOA) bulk  $\text{Bi}_2\text{Te}_3$ , its ZT monotonically increases with temperature and reaches a maximum value of 1 at 400 K followed by a decreasing value at higher temperature; it can be seen that the ZT of nanowires increases dramatically with temperature, and reaches 0.9 at 350 K.

#### 4. Conclusions

Bismuth telluride film and nanowires array (embedded in alumina template) were fabricated by potentiostatic electrodeposition. Both materials are slightly Te-rich, n-type  $\text{Bi}_2\text{Te}_3$ , exhibiting preferred orientation in rhombohedral structure. Their Seebeck coefficient decreases linearly from  $-70 \mu\text{V}/\text{K}$  at 300 K with decreasing temperature, showing a diffusive nature of current flow. Electrical resistivity of a single nanowire separated from the array was measured at 300 K, which was then used as reference in determining resistivity of nanowires at other temperatures. Meanwhile, from temperature-dependent thermal diffusivity and heat capacity data, a thermal conductivity value of  $0.75 \text{ W}/(\text{m K})$  was obtained at 300 K. The ZT was calculated to be 0.45 at 300 K and 0.9 at 350 K for  $\text{Bi}_2\text{Te}_3$  nanowires.

**Acknowledgment.** This work was supported by the National Research Council of the Republic of China under Grant No. NSC 97-2120-M-001-007.

#### References and Notes

- (1) Sales, B. C. *Science* **2002**, *295*, 1248.
- (2) Dutta, N. K.; Cella, T.; Brown, R. L.; Huo, D. T. C. *Appl. Phys. Lett.* **1985**, *47*, 222.
- (3) Rowe, D. M., Ed. In *CRC Handbook of Thermoelectric*; CRC Press: New York, 1995.
- (4) Tritt, T. M. *Science* **1999**, *283*, 804.
- (5) Venkatasubramanian, R.; Siivola, E.; Colpitts, T.; O'Quinn, B. *Nature* **2001**, *413*, 597.
- (6) Hicks, L. D.; Dresselhaus, M. S. *Phys. Rev. B* **1993**, *47*, 16631.
- (7) Zou, H.; Rowe, D. M.; Min, G. J. *Cryst. Growth* **2001**, *222*, 82.
- (8) Peranio, N.; Eibl, O.; Nurnus, J. J. *Appl. Phys.* **2006**, *100*, 114306.
- (9) Boulouz, A.; Chakraborty, S.; Giani, A.; Delannoy, F. P.; Boyer, A.; Schumann, J. *J. Appl. Phys.* **2001**, *89*, 5009.
- (10) Miyazaki, Y.; Kajitani, T. *J. Cryst. Growth* **2001**, *229*, 542.
- (11) Sapp, S. A.; Lakshmi, B. B.; Martin, C. R. *Adv. Mater.* **1999**, *11*, 402.
- (12) Martín-González, M.; Prieto, A. L.; Gronsky, R.; Sands, T.; Stacy, A. M. *Adv. Mater.* **2003**, *15*, 1003.
- (13) Martín-González, M.; Snyder, G. J.; Prieto, A. L.; Gronsky, R.; Sands, T.; Stacy, A. M. *Nano Lett.* **2003**, *3*, 973.
- (14) Jin, C.; Zhang, G.; Qian, T.; Li, X.; Yao, Z. *J. Phys. Chem. B* **2005**, *109*, 1430.
- (15) Prieto, A. L.; Martín-González, M.; Keyani, J.; Gronsky, R.; Sands, T.; Stacy, A. M. *J. Am. Chem. Soc.* **2003**, *125*, 2388.
- (16) Xiao, F.; Hangarter, C.; Yoo, B.; Rheem, Y.; Lee, K.-H.; Myung, N. V. *Electrochim. Acta* **2008**, *53*, 8103.
- (17) Martín-González, M. S.; Prieto, A. L.; Gronsky, R.; Sands, T.; Stacy, A. M. *J. Electrochem. Soc.* **2002**, *149*, C546.
- (18) Jessensky, O.; Müller, F.; Gösele, U. *Appl. Phys. Lett.* **1998**, *72*, 1173.
- (19) Yoo, B. Y.; Huang, C.-K.; Lim, J. R.; Herman, J.; Ryan, M. A.; Fleurial, J.-P.; Myung, N. V. *Electrochim. Acta* **2005**, *50*, 4371.
- (20) Parker, W. J.; Jenkins, R. J.; Butler, C. P.; Abbott, G. L. *J. Appl. Phys.* **1961**, *32*, 1679.
- (21) Cape, J. A.; Lehman, G. W. *J. Appl. Phys.* **1963**, *34*, 1909.
- (22) Blumm, J.; Opfermann, J. *High Temp. High Pressure* **2002**, *34*, 515.
- (23) Mishra, S. K.; Satpathy, S.; Jepsen, O. *J. Phys.: Condens. Matter* **1997**, *9*, 461.
- (24) Borca-Tasciuc, D.-A.; Chen, G.; Prieto, A.; Martín-González, M. S.; Stacy, A. M.; Sands, T.; Ryan, M. A.; Fleurial, J. P. *Appl. Phys. Lett.* **2004**, *85*, 6001.
- (25) Lan, Y.; Poudel, B.; Ma, Y.; Wang, D.; Dresselhaus, M. S.; Chen, G.; Ren, Z. *Nano Lett.* **2009**, *9*, 1419.
- (26) Fleurial, J. P.; Gailliard, L.; Triboulet, R. *J. Phys. Chem. Solids* **1988**, *49*, 1237.
- (27) Pecheur, P.; Toussaint, G. *J. Phys. Chem. Solids* **1994**, *55*, 327.
- (28) Horák, J.; Navrátil, J.; Starý, Z. *J. Phys. Chem. Solids* **1992**, *53*, 1067.
- (29) Augustine, S.; Mathai, E. *Semicond. Sci. Technol.* **2003**, *18*, 745.
- (30) Mansfield, R.; Williams, W. *Proc. Phys. Soc. London* **1958**, *72*, 733.
- (31) Singh, M. P.; Bhandari, C. M. *Solid State Commun.* **2003**, *127*, 649.
- (32) Park, M.-A.; Savran, K.; Kim, Y.-J. *Phys. Status Solidi* **2003**, *237*, 500.
- (33) Zhou, J.; Jin, C.; Seol, J. H.; Li, X.; Shi, L. *Appl. Phys. Lett.* **2005**, *87*, 133109.
- (34) Goldsmid, H. J.; Sharp, J. W. *J. Electron. Mater.* **1999**, *28*, 869.
- (35) Snyder, G. J.; Toberer, E. S. *Nat. Mater.* **2008**, *7*, 105.
- (36) Nan, C.-W.; Birringer, R.; Clarke, D. R.; Gleiter, H. *J. Appl. Phys.* **1997**, *81*, 6692.
- (37) Li, D.; Prieto, A. L.; Wu, Y.; Martín-González, M. S.; Stacy, A.; Sands, T.; Gronsky, R.; Yang, P.; Majumdar, A. *The 21st International Conference on Thermoelectrics*, August 25–29, 2002, Long Beach, CA, Symposia Proceedings, No. 2002ICT, Piscataway, NJ, 2002; p 333.
- (38) Moore, A. L.; Pettes, M. T.; Zhou, F.; Shi, L. *J. Appl. Phys.* **2009**, *106*, 034310.